JOINT INSTITUTE FOR LABORATORY ASTROPHYSICS

UNIVERSITY OF COLORADO
BOULDER, COLORADO 80309

UNIVERSITY OF COLORADO

NATIONAL BUREAU OF STANDARDS

SEMIANNUAL REPORT

RESEARCH IN LASER PROCESSES

Research Sponsored by
Advanced Research Projects Agency
and
Office of Naval Research

ARPA Order No. 2683, Amendment 4
Program Code No. 7E20
Contractor: University of Colorado
Effective Date of Contract: July 1, 1975
Contract Expiration Date: Sep. 30, 1977
Amount of Contract $310,000
Period Covered: July 31, 1976 to
January 31, 1977

Contract No. N00014-76-C0123
Principal Investigators:
A.V. Phelps
Telephone: (303) 492-7850
A.C. Gallagher
Telephone: (303) 492-7841
Scientific Officer: Director,
Physics Program, ONR
Short Title of Work: Laser Processes

July 25, 1977

Cable Address: JILA

Telephone Number: 492-7789

Unclassified

SECURITY CLASSIFICATION OF THIS PAGE *(When Data Entered)*

REPORT DOCUMENTATION PAGE

READ INSTRUCTIONS BEFORE COMPLETING FORM

1. REPORT NUMBER: None
2. GOVT ACCESSION NO.
3. RECIPIENT'S CATALOG NUMBER

4. TITLE *(and Subtitle)*: Semiannual Report
(6) Research in Laser Processes.

5. TYPE OF REPORT & PERIOD COVERED: (9) Semiannual Rept. 1 Aug 76 - 31 Jan 77,

6. PERFORMING ORG. REPORT NUMBER

7. AUTHOR(s): (10) A.V. Phelps, A.C. Gallagher

8. CONTRACT OR GRANT NUMBER(s): (15) N00014-76-C-0123, ARPA Order-2683

9. PERFORMING ORGANIZATION NAME AND ADDRESS
University of Colorado
Joint Institute for Laboratory Astrophysics
Boulder, CO 80309

10. PROGRAM ELEMENT, PROJECT, TASK AREA & WORK UNIT NUMBERS
NR012-512/~~10-6-7~~, Code 421
ARPA Ord. No. 2683, Amd. ~~1~~,
Prog. Cd. 7E20

11. CONTROLLING OFFICE NAME AND ADDRESS
Office of Naval Research
Department of the Navy
800 North Quincy St., Arlington, VA 22217

12. REPORT DATE: (11) 25 July 77

13. NUMBER OF PAGES: ~~32~~ (12) 35p.

14. MONITORING AGENCY NAME & ADDRESS *(if different from Controlling Office)*

15. SECURITY CLASS. *(of this report)*: Unclassified

15a. DECLASSIFICATION/DOWNGRADING SCHEDULE

16. DISTRIBUTION STATEMENT *(of this Report)*

APPROVED FOR PUBLIC RELEASE; DISTRIBUTION UNLIMITED

17. DISTRIBUTION STATEMENT *(of the abstract entered in Block 20, if different from Report)*

18. SUPPLEMENTARY NOTES

19. KEY WORDS *(Continue on reverse side if necessary and identify by block number)*

Laser, processes, sodium vapor, rare gas, electrical discharge, high pressure, molecules, metastables.

20. ABSTRACT *(Continue on reverse side if necessary and identify by block number)*

Numerical models of electric discharges in Na-Xe mixtures have been developed in order to examine the utility of this system for high efficiency, high power, visible lasers. Although the models are incomplete, metal vapor-rare gas discharges continue to appear promising for this application. The detailed models of the time development of the cathode fall of a high pressure discharge have been completed. Measurements and analyses of rate coefficients for electron excitation of O_2 (continued on reverse side...) and N_2 to metastable states)

DD FORM 1 JAN 73 1473 EDITION OF 1 NOV 65 IS OBSOLETE

Unclassified (cont over)

SECURITY CLASSIFICATION OF THIS PAGE *(When Data Entered)*

192900

(cont'd p 1473A)

are being studied.

to the $b^1\Sigma_g^+$ metastable state have been completed. Measurements of excitation of N_2 to the $A^3\Sigma_u^+$ metastable state have been initiated. Measurements have been completed of the spectral intensity of scattered light at wavelengths near the resonance line when Na vapor is illuminated by white light. The agreement with theory is good over a wide range of Na densities and added N_2 densities.

SEMIANNUAL REPORT

This Semiannual Report contains descriptions of work carried out under ONR Contract No. N00014-76-0123 and ARPA Order No. 2683, and Amd. 4, and covers the period from 1 August 1976 to 31 January 1977. Section I is the Semiannual Report Summary while Sections II-V are more detailed descriptions of work carried out under the four projects supported by this contract.

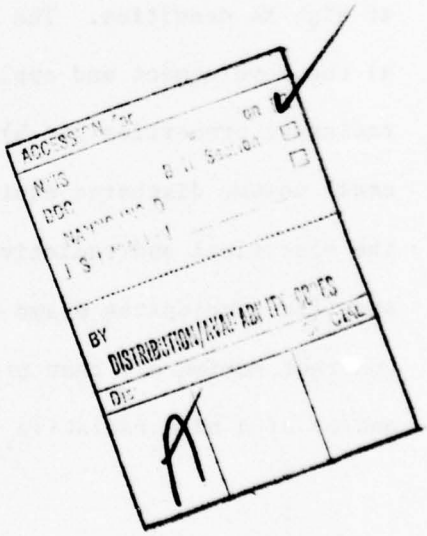

I. SEMIANNUAL REPORT SUMMARY

The four projects being carried out in the area of Laser Processes under this contract are summarized below. More detailed discussions are given in Sections II through V of this report.

(1) Metal Vapor-Rare Gas Discharges.

Several metal vapor-rare gas molecules have been proposed as the active media for high efficiency, high power excimer lasers operating at near visible wavelengths. Our previous research in this area had been directed primarily toward the measurement of the stimulated emission and absorption coefficients for some of these molecules. The present work is a more detailed evaluation of the potential for laser use of one of the more promising of these molecules, i.e., the NaXe molecule. In order to take advantage of the high quantum efficiency inherent in these excimer systems, i.e., greater than 80%, it is desirable to excite the associated atomic levels as efficiently as possible. We believe that electric discharge excitation with its low mean electron energies offers the best possibility for efficient excitation and so have initiated the present investigation of electric discharges in mixtures of Na and Xe at high Xe densities. The effort covered by this report includes a) the development and application of models of the discharge and its radiative properties and b) the construction and initial operation of a small volume discharge equipped with apparatus for the measurement of the electrical and radiative properties of the discharge. The principal specific conclusions drawn from the modeling calculations during this contract period are that presence of significant excited state populations and/or of a high radiative flux level drastically changes the electron energy

balance and the degree of ionization, that the earlier indication of a large reduction Na_2 density by electron collisional dissociation is correct, and that the model is incomplete and will have to be extended to include at least several more excited states of the sodium atom. The general conclusion is that discharge excited metal vapor-rare gas systems continue to appear to be viable candidates as high efficiency, high power lasers for near visible wavelengths.

(2) Stability of Discharges in Weakly Ionized Gases.

The technical problem being investigated is the optimization of the use of electrical energy for the production of excited molecules in electrically excited gas lasers. In particular, the efficient use of electrical excitation in gas lasers requires that the discharge remain diffuse as the density of the excited atoms and molecules is raised as high as possible, i.e., that the discharge not form a constricted channel or arc. There is evidence that arcing in lasers originates in or near the region of very high energy input at the cathode, known as the cathode fall. During this report period we have essentially completed our calculations of the time development of the cathode fall region of a high pressure discharge and have initiated an analysis of published experimental data based on the scaling laws derived from the theory.

(3) Electron Excitation of Molecular Metastables.

The electron excitation of molecular metastables in an electrical discharge can be an efficient means of producing high excited state densities in gas lasers. During this report period we have extended the measurements of electron excitation rate coefficients for the $O_2(b^1\Sigma_g^+)$ metastable state to excitation in mixtures of O_2 and N_2 and have initiated measurements of electron

rate coefficients for the $A^3\Sigma_u^+$ state of N_2 in pure N_2. The $O_2(b^1\Sigma)$ measurements in O_2-N_2 mixtures confirm our results in pure O_2, i.e., the measured total excitation rate coefficients at mean electron energies of about 2 eV are as much as a factor of three larger than expected on the basis of previously available data.

(4) Scattering and Transport of Resonance Radiation in Gases.

The technical problem considered here is the measurement of the transport and scattering of resonance radiation emitted by metal vapors so as to obtain the rates of radiative and non-radiative energy loss by excited atoms in excimer lasers, etc. The measurements of the spectral intensity of scattered radiation under white light illumination have been completed and initial comparisons have been made with theory. These measurements confirm the loss of excited Na atoms by excitation transfer to Na_2 molecules. The integrated scattered intensities confirm the validity of theoretical model at low ($<10^{14}$ atom/cm^3) and at high ($>10^{15}$ atom/cm^3). The discrepancies at intermediate Na densities may be caused by the approximate manner in which the theory treats coherently scattered radiation. Also, during this report period experiments were initiated in which a dye laser will be used to excite the Na resonance state near line center so as to emphasize the effects of the non-radiative excitation transfer process.

II. METAL VAPOR-RARE GAS DISCHARGES

Drs. H. Rothwell, R. Shuker, and A. Gallagher and Mr. D. Leep.

The objective of this project is to determine whether metal vapor-rare gas discharges can be operated so as to produce the degree of metal vapor-rare gas excimer excitation required for high power visible laser opeationn. The project includes experimental measurements and theoretical models of the properties of Na-Xe discharges at rare gas pressures up to about 10 atm.

The Na-Xe mixture is chosen because we have more of the data needed for a meaningful model[1] and because this mixture might yield a high power visible excimer laser. In particular, our previous calculations indicate that potentially ruinous effects,[2] such as absorption by ground state Na_2, are not important.[1] The following discussion summarizes our modeling efforts up to the date of this report. The portion of the work carried out under this contract includes a) the development and application of procedures for the iteration of the solutions for the electron energy distribution and for the populations of the excited states, ions, and electrons; b) the inclusion of the effects of stimulated emission and of the intercavity flux in the model; and c) the effects of the addition of a third excited state on the discharge gain, etc.

The A-X bands of alkali-noble gas excimers and alkali-dimers have been proposed for high-power, efficient lasers and gain cells in the 650-1300 nm wavelength region.[2,3] The excited states of these excimers are weakly bound compared to those of the rare gas molecules,[4] but net gain was predicted with a few percent excited alkali atoms due to a strongly repulsive ground state. The alkali dimers also yielded net gain on the A-X bands at a few percent excitation, due to displaced A and X state potentials which yield emission centered at longer wavelengths than absorption.

A typical gas mixture considered here is 10^{15} - 10^{17} atoms/cm^3 of alkali, with a few percent bound as dimers, and about 10^{20} atoms/cm^3 of noble gas to act as a heat sink and a constituent of the excimer molecule. Since the excimer and dimer bands are associated with the first excited alkali state, while the noble gas excited states are at much higher

energies, electric discharge excitation is an attractive possibility. Simple models of a laser utilizing K-Xe have been given by Palmer[5] using Maxwellian electron-energy distributions f(u) and a limited set of population rate equations. Schlie[6] has shown that at low fractional ionization the rapidly decreasing non-Maxwellian tail of f(u) allows efficient excitation of the lasing alkali state rather than the noble gas. The present work has modeled this laser by solving self-consistently the Boltzmann equation for f(u) and an extensive set of rate equations for the various excited and ionized species densities. We assume a homogeneous self-sustained discharge at fixed E/N. The questions of instabilities or constrictions are being studied experimentally in this laboratory.[7]

We have modeled a Na-Xe mixture since the Na_2 and NaXe A-X bands are fairly well understood,[2,8,9] many electron-Na cross sections are available,[1,10,11] and the population inversion obtained with Na-Xe is higher than with Na and other noble gases. We report here calculations for the case of [Na] = 3.5×10^{16} cm^{-3}, [Xe] = 2.7×10^{20} cm^{-3}, T = 760 K, and E/N = 8×10^{-18} V cm^2, where [ ] indicates species density, T is the gas temperature, E is the applied electric field, and N is the total gas density. Figure 1 shows the Na, Na_2, and NaXe levels included in the model, as well as the most important processes. Due to close coupling by electron collisions the Na 4S and 3D levels are combined into a "4S" level, and the $Na_2(A^1\Sigma_u^+)$ and $Na_2(a^3\Pi)$ are combined into an A' level composed of $1/7(A^1\Sigma)$ state and $6/7(a^3\Pi)$ state.[2] Electron momentum transfer, excitation, deexcitation, ionization, and dissociative recombination are included. The calculation starts with an electron density of $n_e = 10^{11}$ cm^{-3} and typically reaches steady state in a few microseconds. At steady-state

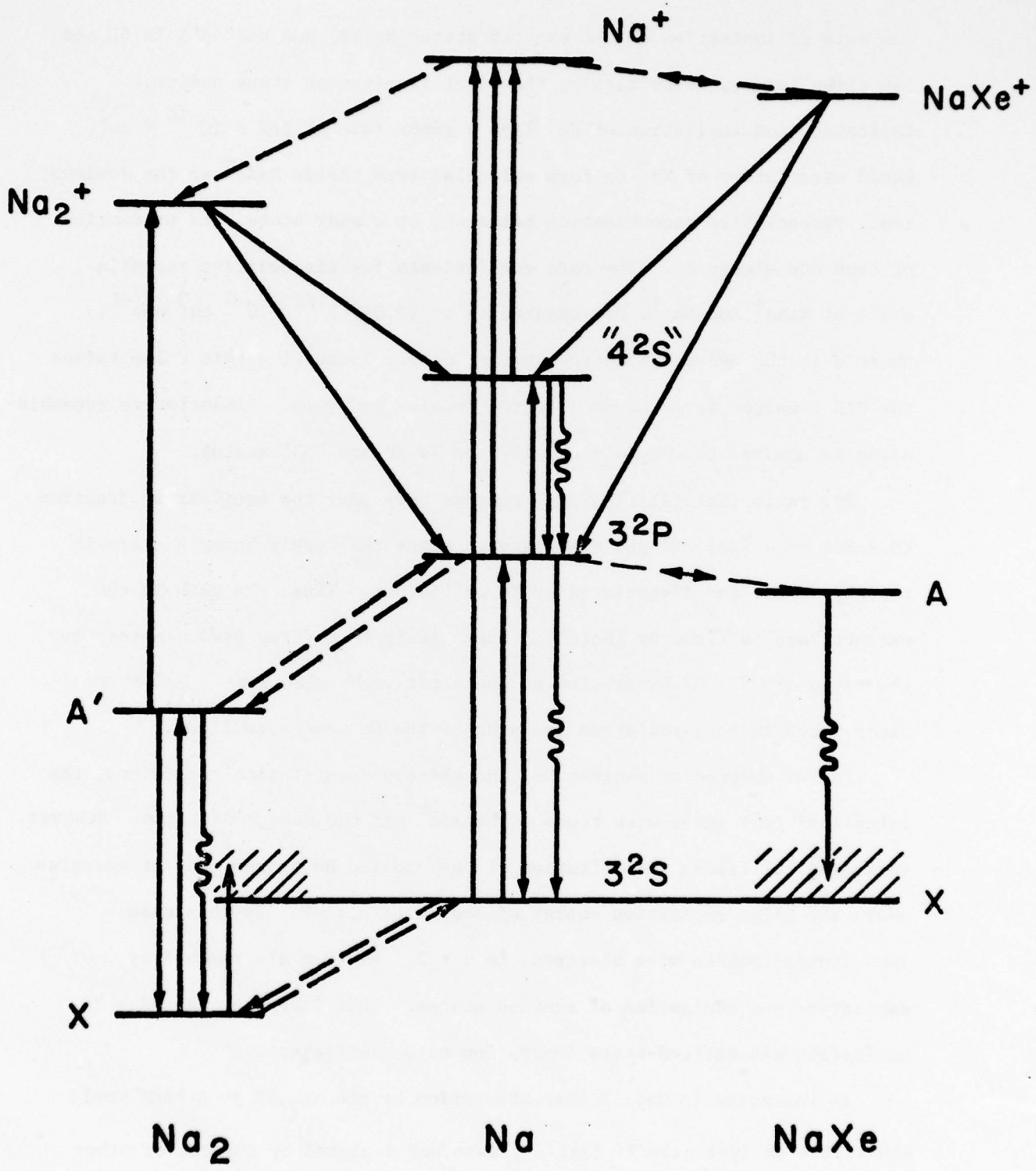

Fig. 1. Energy levels and major processes in model of Na-Xe discharge.

the rate of ionization of the excited states Na(3P) and Na("4S") is 60 and 140 times larger, respectively, than that from ground state sodium. Excitation and ionization of Xe plays a minor role at $E/N < 10^{-16}$ V cm^2. Rapid association of Na^+ to form molecular ions yields $NaXe^+$ as the dominant ion. Dissociative recombination balances, at steady state, the production of ions and electrons. The rate coefficients for dissociative recombination of $NaXe^+$ and Na_2^+, are assumed to be $(0.04/\bar{u})^{1/2} \times 10^{-7}$ cm^3 sec^{-1}, where $\bar{u}$ is the average electron energy in eV. Increasing this value raises the E/N required for a given electron density and gain. Dissociative recombination is assumed to populate equally the Na 3P and "4S" states.

The ratio [NaXe(A)]/[Na(3P)] remains very near the equilibrium fraction (0.2 for this [Xe] and gas temperature) since the weakly bound A state is rapidly formed and dissociated by Xe collisions. Thus, the gain in the excimer band is fixed by [Na(3P)], which is in turn fixed predominately by the ratio of 3S → 3P excitation to deexcitation by electrons. Radiative decay rates include radiation trapping of the Na resonance lines.

In the absence of excited Na, and thereby deexcitation collisions, the calculated f(u) agree with those of Schlie[6] for the same conditions. However, including collisional deexcitation of the excited Na raises f(u) at energies above the first excitation energy of sodium at 2.1 eV. In this case deexcitation shifts more electrons to u > 2.1 eV than are removed by excitation and ionization of excited states. This increases the 3S → 3P excitation and excited-state ionization rate coefficients.

It was noted in Ref. 2 that absorption by the Na_2, X to A band could cancel the excimer gain if [Na_2(X)] were not depleted by thermal or other mechanisms. One of the principal conclusions of the present study is that [Na_2(X)] is greatly depleted by electron collisional dissociation at the

steady-state n_e appropriate for high-power operation. This dissociation process occurs via electron collision excitation from $X^1\Sigma_g$ to the repulsive $x^3\Sigma_u$ state, which dissociates to two Na(3S) atoms. The identical process has been measured[12] and calculated[13] for H_2 dissociation. The estimated Na_2 cross section is obtained by multiplying the measured H_2 cross section by ρ^2 and dividing its energy scale by ρ, where ρ is the ratio of the excitation thresholds for H_2 and Na_2. This form of scaling has been found accurate in many cases.[14-16] A similar process with twice the cross section is assumed to deplete the $Na_2(A')$ state. Depletion resulting from gas heating and electron-induced vibrational excitation are not included. Thus the actual depletion should exceed that calculated

For the above total Na and Xe densities and E/N, the rate equations without inclusion of stimulated emission yield steady-state values of $n_e = 3 \times 10^{15}$ cm^{-3}, $[Na(3P)] = 3 \times 10^{15}$ cm^{-3}, $[Na("4S")] = 4 \times 10^{14}$ cm^{-3}, $[Na_2(X)] = 9 \times 10^{13}$ cm^{-3}, $[Na_2(A)] = 1/7 \times [Na_2(A')] = 4 \times 10^{12}$ cm^{-3}, $[Na^+] = 10^{14}$ cm^{-3}, $[Na_2^+] = 10^{14}$ cm^{-3}, and $[NaXe^+] = 3 \times 10^{15}$ cm^{-3}. The resulting steady-state stimulated emission g_ν and absorption coefficients k_ν are given in Fig. 2. These curves are based on the normalized k_ν and g_ν coefficients given in Refs. 2 and 8, except that the radiative transition probability for the Na_2 A-X band is twice[17] that used in Ref. 2. The $Na_2(X)$ absorption shown in Fig. 2 is smaller by a factor of 20 than that predicted by thermal equilibrium. A net gain of $10^{-1} - 10^{-3}$ cm^{-1} is indicated for the excimer band. The Na_2 A-X band has only $\sim 10^{-3}$ cm^{-1} gain in this figure, but can be considerably larger at lower E/N and n_e, where less depletion occurs. The excimer transition is homogeneously broadened on a 10^{-10} sec time scale, as determined by measured excimer dissociation rates.[18] Thus, the laser could operate at any wavelength from 680-900 nm.

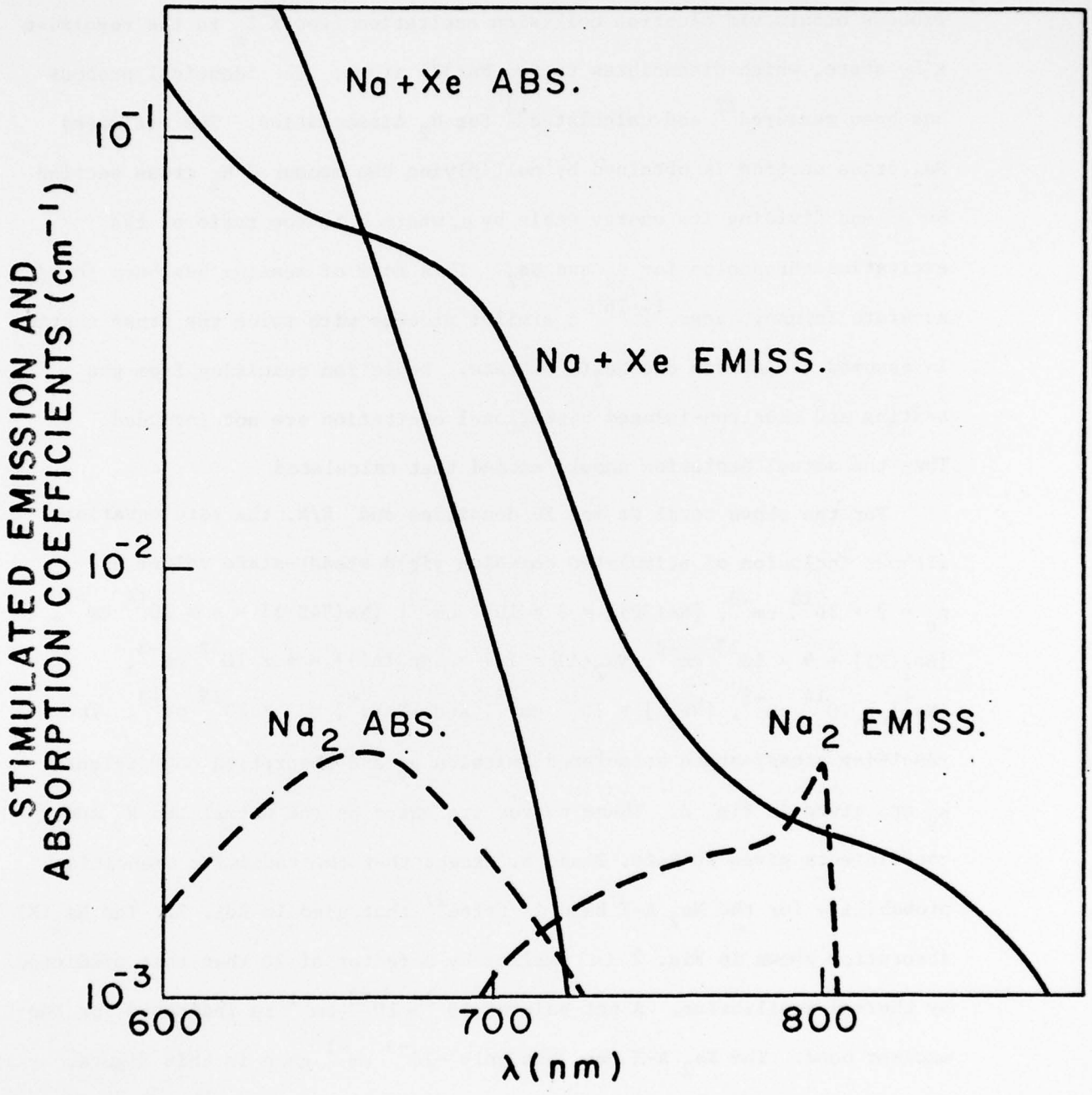

Fig. 2. Calculated stimulated emission and absorption coefficients for $[Na] = 3.5\times10^{16}$ cm^{-3}, $[Xe] = 2.7\times10^{20}$ cm^{-3}, T = 760 K, and $E/N = 8\times10^{-18}$ $V\text{-}cm^{2}$. As discussed in the text the result of this preliminary model must be used with caution pending a thorough investigation of the effects of the addition of higher excited states.

The calculations show that the homogeneous discharge has a positive volt-ampere characteristic with a resistivity of about 20 Ω-cm. This behavior is the result of a balance between ionization via excited Na atoms, which increases approximately linearly with electron density, and the loss of electrons and ions, which is proportional to the square of the electron density.

The rate equations have also been solved with the inclusion of stimulated emission to evaluate the potential laser power and efficiency. As the radiative flux is increased E/N must be raised so as to maintain sufficient excited state and electron density. Thus, Fig. 3 shows the dependence of the net gain at λ = 700 nm on the cavity power at steady-state for $E/N = 1 \times 10^{-17}$ V cm^2. It also shows the corresponding radiative power output and electrical power input. The solid curves of Fig. 3 show calculations for the full value of the estimated cross sections for electron impact dissociation of the $Na_2(X)$ and $Na_2(A')$ states, while the dashed curves are for one tenth of these cross sections. The presence of a high cavity flux causes bleaching of the $Na_2(A-X)$ band reducing the absorption.

As an example of laser characteristics predicted from the calculations of Fig. 3, consider the conditions for the case of the full Na_2 dissociation cross section and the maximum radiant power output. Using the spatially uniform flux approximation[19] for a laser oscillator with a single transmitting mirror we find that if the laser were 50 cm long and a 50% transmission output mirror were used, the output power would be about 1.5 MW/cm^2 and the overall efficiency would be about

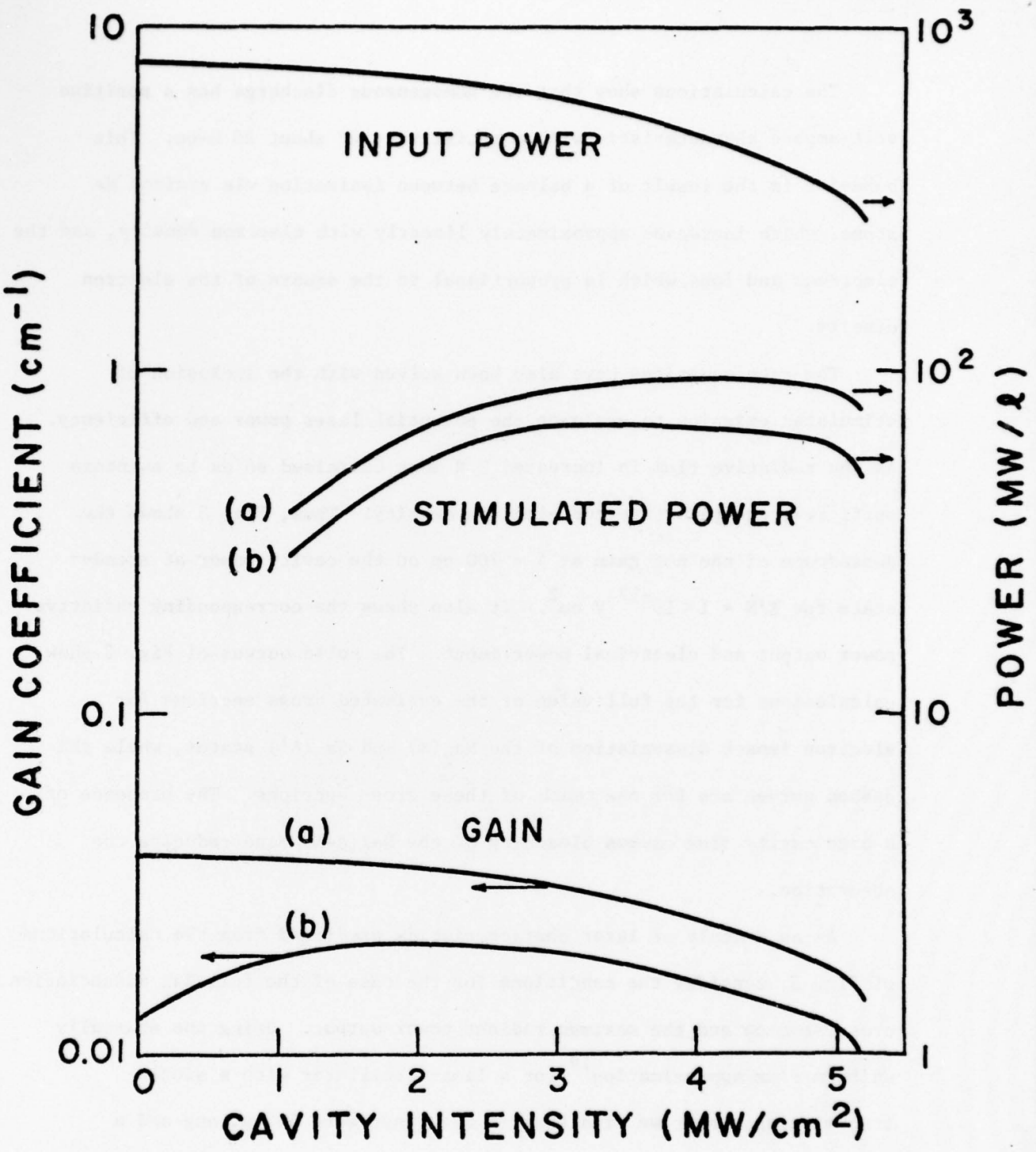

Fig. 3. Calculated gain and power output vs. cavity flux at 700 nm for Na-Xe discharge. See text for remarks on the validity of this preliminary model.

10%. The intercavity flux would be about 5 MW/cm^2 and the input power would be 30 MW/ℓ. The specific heat of the Xe results in a gas temperature rise of 100 K/μsec, so that the laser pulse might terminate after a few microseconds of operation. These conditions have not yet been optimized with respect to the output coupling, the [Na]/[Xe] ratio, the [Xe] density or E/N.

This initial modeling of electric discharge excitation of the Na-Xe excimer indicates that this system could yield an efficient, tunable, high-power laser or gain cell operating near 700 nm. Obviously a number of practical problems remain to be addressed, e.g., the optical quality of the medium and the practical operation of Na-Xe discharges at the high E/N of these models. The principal uncertainty in the model appears to be whether the use of two or three excited states adequately represents the effects of multistep ionization.[20] Results obtained subsequent to this report period show that a correct model will somehow include the effects of a large number of excited states.

The experimental portion of this effort included the design and construction of an improved high temperature discharge cell, the calibration of the optical system for absolute intensity measurements, and two preliminary spectral scans at relatively low discharge current densities. Figure 4 shows the spectral distribution of radiation emitted at [Na] = 7.5×10^{15} cm^{-3}, [Xe] = 4.6×10^{19} cm^{-3} and $J_{pk} \approx 100$ A/cm^2. The dashed curves show the contributions of the NaXe (A→X) band and the Na_2 (A→X) band. Note that at these high current densities the Na_2 band intensity is much lower than expected for an equilibrium ratio of Na_2 to Na, i.e., Na_2 depletion is large as predicted by our model for low current densities.[9] During the next report period the absolute intensities of the various bands and lines will be used to calculate Na and NaXe excited state densities for comparison with discharge models and to predict discharge characteristics at higher power densities.

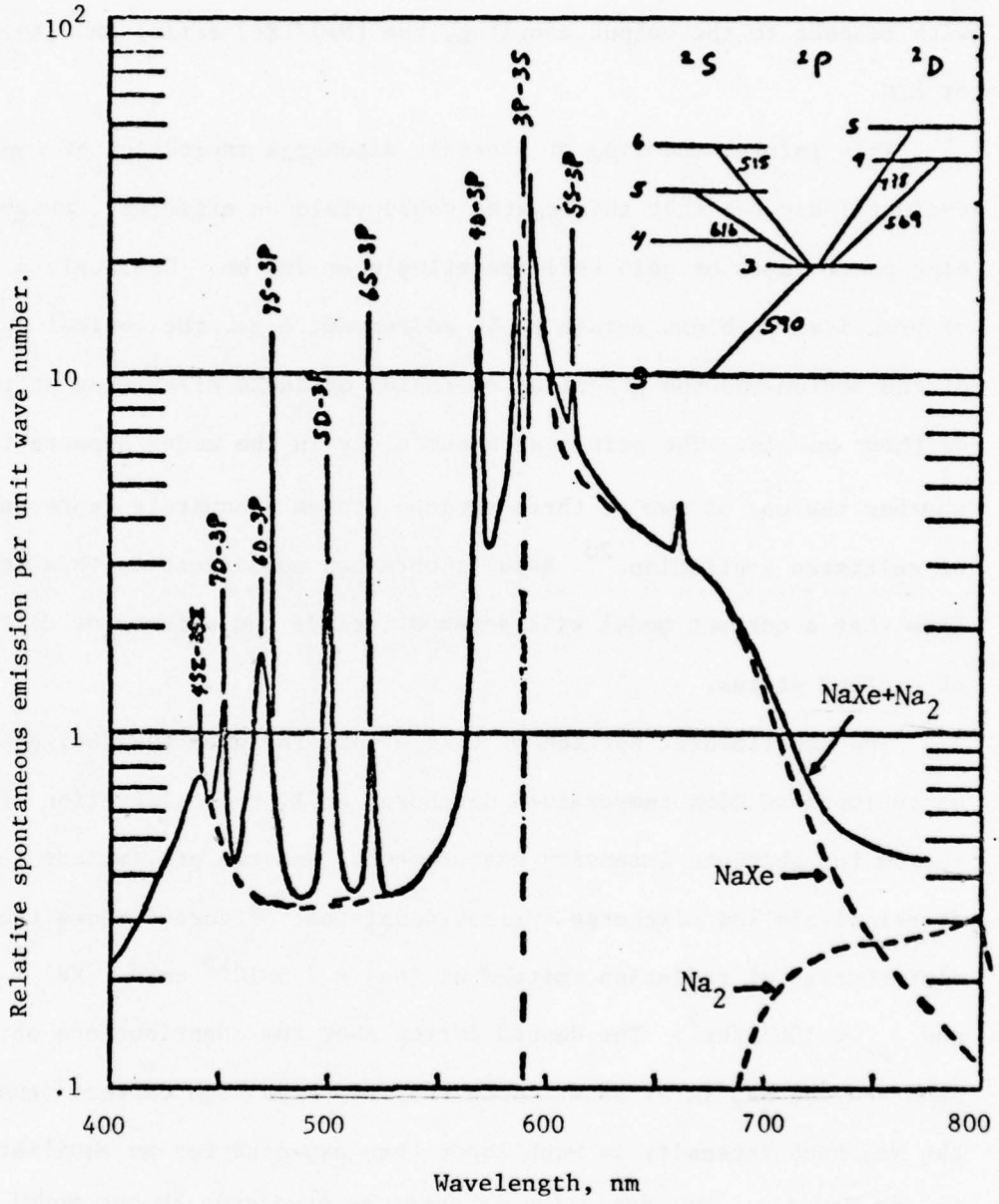

Fig. 4. Experimental spectral intensity distribution from Na-Xe discharge for [Na] = 7.5×10^{15} cm^{-3}, [Xe] = 4.6×10^{19} cm^{-3} and $I_{pk} \approx 13.4$ A.

III. STABILITY OF DISCHARGES IN WEAKLY IONIZED GASES

Drs. H.-C. Chen and A. V. Phelps

The objective of this theoretical investigation of the growth of instabilities in weakly ionized gas discharge is to develop quantitative techniques for the prediction of conditions for formation of the arcs which limit the power output from high power laser systems. The availability of such techniques would greatly aid the optimization of high power lasers currently under development and would greatly improve the reliability of the design of scaled-up versions of these lasers. During this contract period we have essentially completed our development of techniques for the detailed calculation of the growth of the cathode fall region of a glow discharge. The model described in detail below uses one dimensional solutions of the continuity equations for electrons and positive ions and Poisson's equation. The electron and ion transport coefficients and the ionization and recombination coefficients were based on experimental measurements for helium, which is used as the principal constituent in most electric discharge lasers. These coefficients are readily modified to allow the modeling of gas mixtures. Thus far we have not modeled the cathode fall for discharges using attaching gases. These calculations represent improvements over previous analyses in that the earlier work omitted electron diffusion[21,23] and/or presented only very limited results.[22,23]

A. Theory

(1) Basic Equations

The electron and positive ion rate equations, Poisson's equation, and experimental transport and rate coefficients are used for tracing the growth in time and space of a one-dimensional helium discharge where the electric field is distorted by the space charge of the electrons and ions. The continuity equation for electrons is

$$\frac{\partial n_e}{\partial t} + \nabla \cdot (n_e \underset{\sim}{u}) = \nu n_e - \alpha n_e n_+ \ , \tag{1}$$

where n_e and n_+ are the electron and positive ion densities, t is the time, ν is the ionization coefficient, and α is the recombination coefficient. The electron velocity $\underset{\sim}{u}$ can be expressed in terms of drift and diffusion velocity as

$$\underset{\sim}{u} = - \mu \underset{\sim}{E} - \frac{\nabla(n_e D)}{n_e} \ , \tag{1a}$$

where $\underset{\sim}{E}$ is the electric field, D and μ are the diffusion and mobility coefficients of the electrons, respectively.

The continuity equation for positive ions is

$$\frac{\partial n_+}{\partial t} + \nabla \cdot (n_+ \underset{\sim}{u}_+) = \nu n_e - \alpha n_e n_+ . \tag{2}$$

The ion velocity $\underset{\sim}{u}_+$ can be expressed as

$$\underset{\sim}{u}_+ = \mu_+ \underset{\sim}{E} \ , \tag{2a}$$

where μ_+ is the mobility of positive ions. The diffusion of the ions has been neglected because of their heavy mass.

Poisson's equation describing the space-charge-distorted fields is

$$\frac{\partial E}{\partial z} = \frac{e}{\varepsilon_o} (n_+ - n_e) \ , \tag{3}$$

where e is the electronic charge, ε_o is the permittivity of free space and z is the position in the axial direction.

The coefficients D, ν, α, u_+ and μ must be taken from the experimental measurement or electron transport coefficient calculations. For atomic helium they are expressed in terms of the ratio of electric field to gas density E/N and shown in Eq. (8) of Reference 24.

An allowance has been made for the time required for electrons emitted from the cathode to attain the ionization rate appropriate to the local E/N value by requiring the electrons to pass through a potential of 40 V before ionization begins. See Druyvesteyn and Penning.[25]

(2) Boundary Conditions

At the cathode, secondary electrons are produced by the bombardment of ions and photons

$$\Gamma_e(0) = \gamma_+\Gamma_+(0) + \gamma_p \ \Gamma_{photon}, \tag{4}$$

where Γ_i represents the flux of various particles i. γ_+ and γ_p are the secondary coefficients representing the probability of the production of secondary electrons at the cathode per incident positive ion or photon. The effect of photons is to enhance the production of secondary electrons and speed up the formation of the cathode fall at the early times in discharge.

At the anode, we have zero density for both electrons and ions

$$n_e(d) = n_+(d) = 0 \quad . \tag{5}$$

The voltage across the discharge gap is V so that

$$\int_0^d Edz = V \quad . \tag{6}$$

Equation (1) is a second order partial differential equation with two boundary conditions. Equations (2) and (3) are first order partial differential equations with one boundary condition. Therefore, we have a complete set of three partical differential equations that can be solved numerically for the three unknowns n_e, n_+ and E. A Crank-Nicholson finite difference scheme[26] which is implicit both in time and space has been used and a predictor-corrector step has been added to take into account the nonlinear coefficients in the equations. Use of nonuniform spatial step-sizes has been found very effective in studying the time development of the boundary layer in the cathode fall region.

B. Results

As in a double discharge laser, an initial electron and ion density which varies smoothly with z and has a peak value of 3×10^{10} cm^{-3} is assumed. This initial ionization is shown in Fig. 5. Calculations are shown for a gap length of 2 cm, a helium density N of 3×10^{19} cm^{-3}, and $E/N = 1.8 \times 10^{-16}$ V cm^2. A γ_+ of .09 has been chosen and the effect of photons has been neglected in the calculations shown.

Figure 6 shows that the electric field is reduced by charge separation in the region of maximum initial ionization at the early time. The density difference between electrons and ions is very small in the plasma region. The field near cathode increases as the electrons are swept toward the anode. The field increases near the cathode until it becomes high enough to cause an ionization wave to move toward the cathode. This is illustrated in Fig. 7 for two different times. Note that the figures show only the small region within .03 cm of the cathode. The electric field near cathode becomes high and forms the cathode fall. At t = 0.13 μsec, as shown in Fig. 8, the current density is 10 amperes/cm^2 and the thickness of cathode fall is about 2×10^{-3} cm.

The sequence of electric field and charge distributions in the cathode fall region is essentially independent of gap length with the time scale decreasing from ~200 ns for a 3 mm gap and 100% overvoltage to ~60 ns for a 7 cm gap and 50% overvoltage.

Figure 9 shows the growth of the electron and ion current density through the gap as calculated using the relation

$$JV = e\int_o^d (n_e u + n_+ u_+ + \frac{\varepsilon_o}{2}\frac{\partial}{\partial t}\int_o^d E^2 dz \ .$$

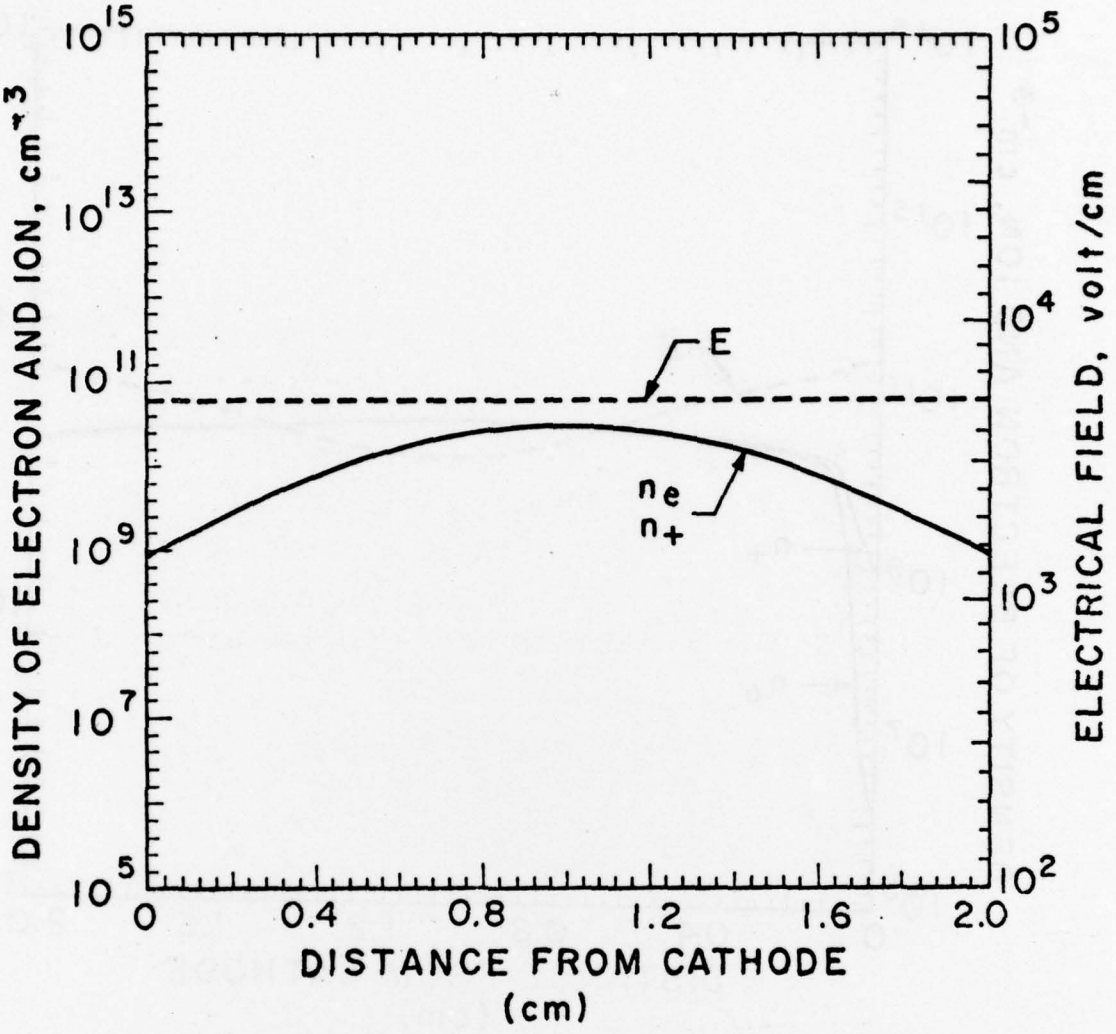

Fig. 5. Initial electron and ion densities and electric field.

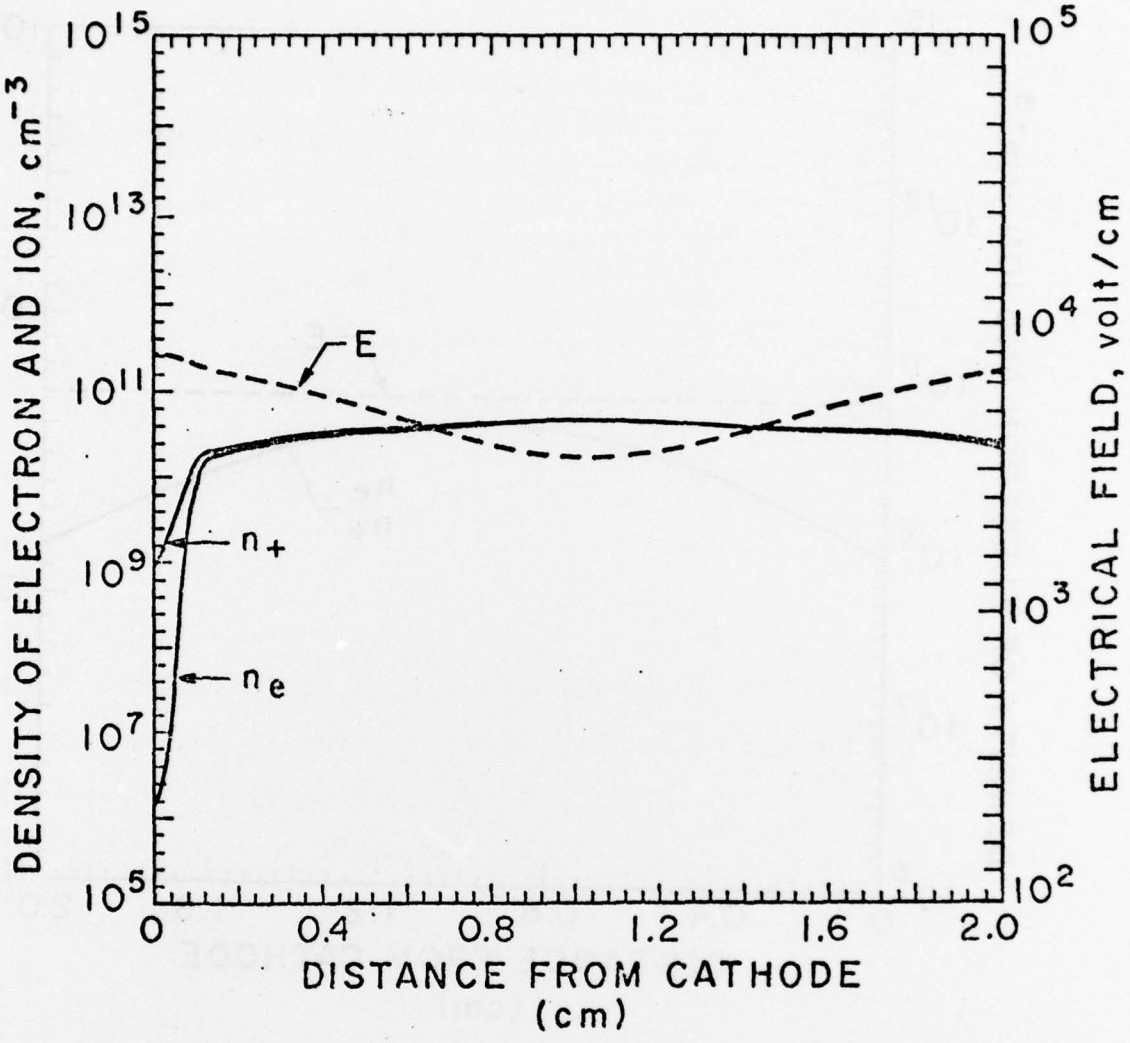

Fig. 6. Electron and ion densities and electric field at 0.02 μsec after initiation of discharge, showing depletion of electrons near cathode by flow toward anode.

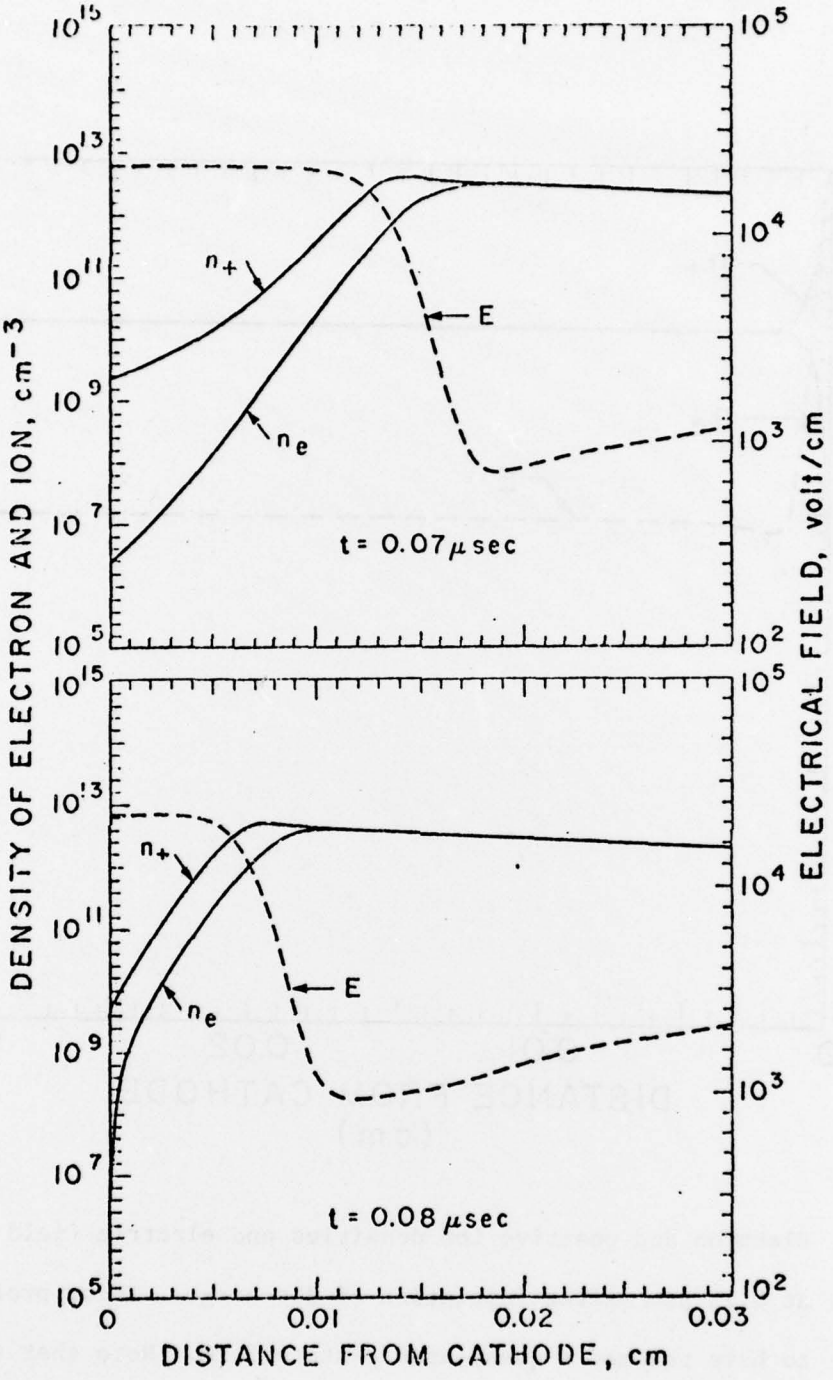

Fig. 7. Electron and ion densities and electric field near the cathode at 0.07 and 0.08 μsec after initiation of discharge. Note the motion of the ion density peak and the sheath boundary toward the cathode.

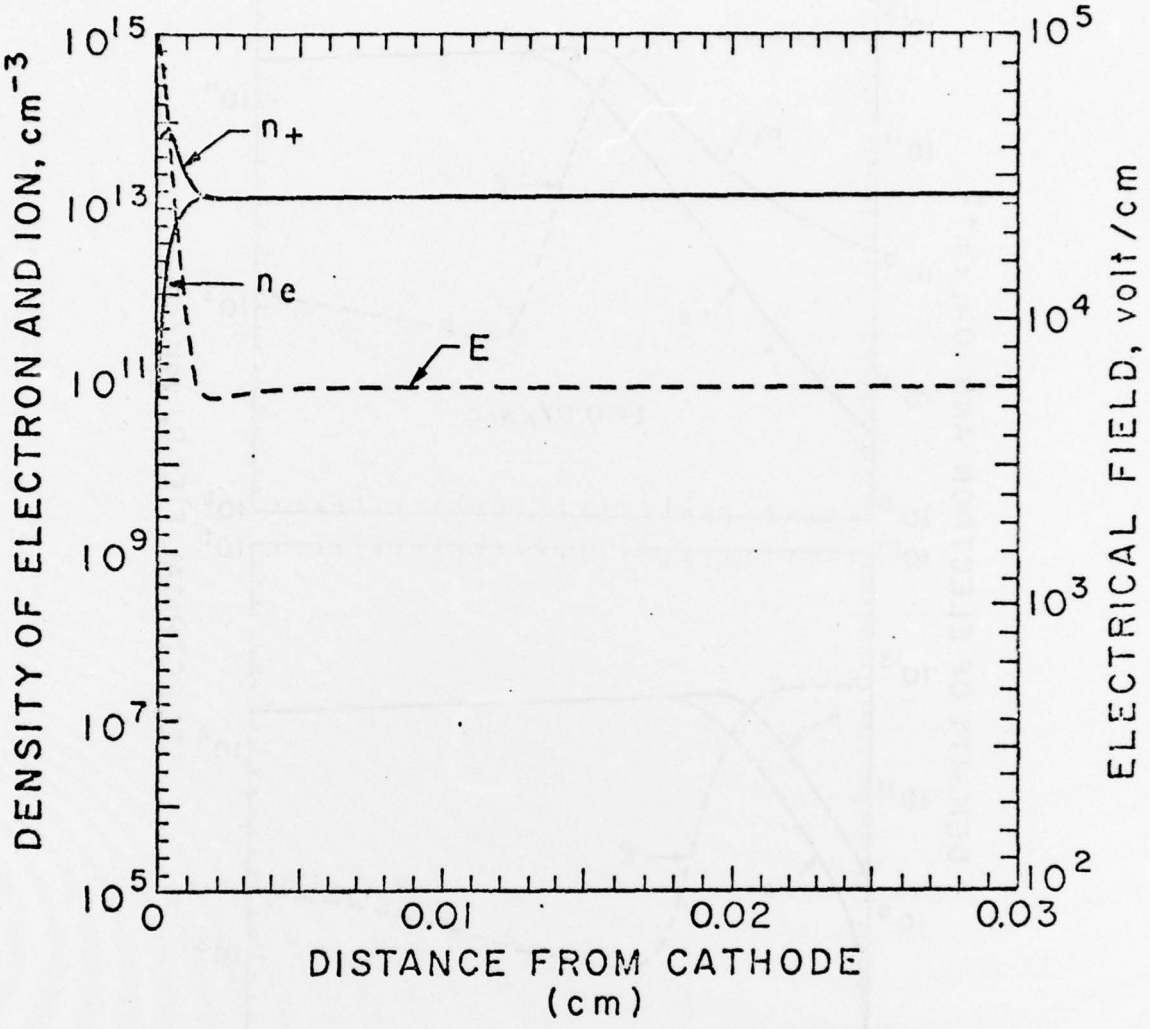

Fig. 8. Electron and positive ion densities and electric field near cathode at 0.13 μsec after initiation of discharge. These profiles appear to have reached a quasi-steady-state form. Note that the calculations in Figs. 5-8 were carried out without delayed onset of ionization. These curves are very similar to those obtained with the delay except that in the present case the sheath is thinner and the voltage drop is smaller.

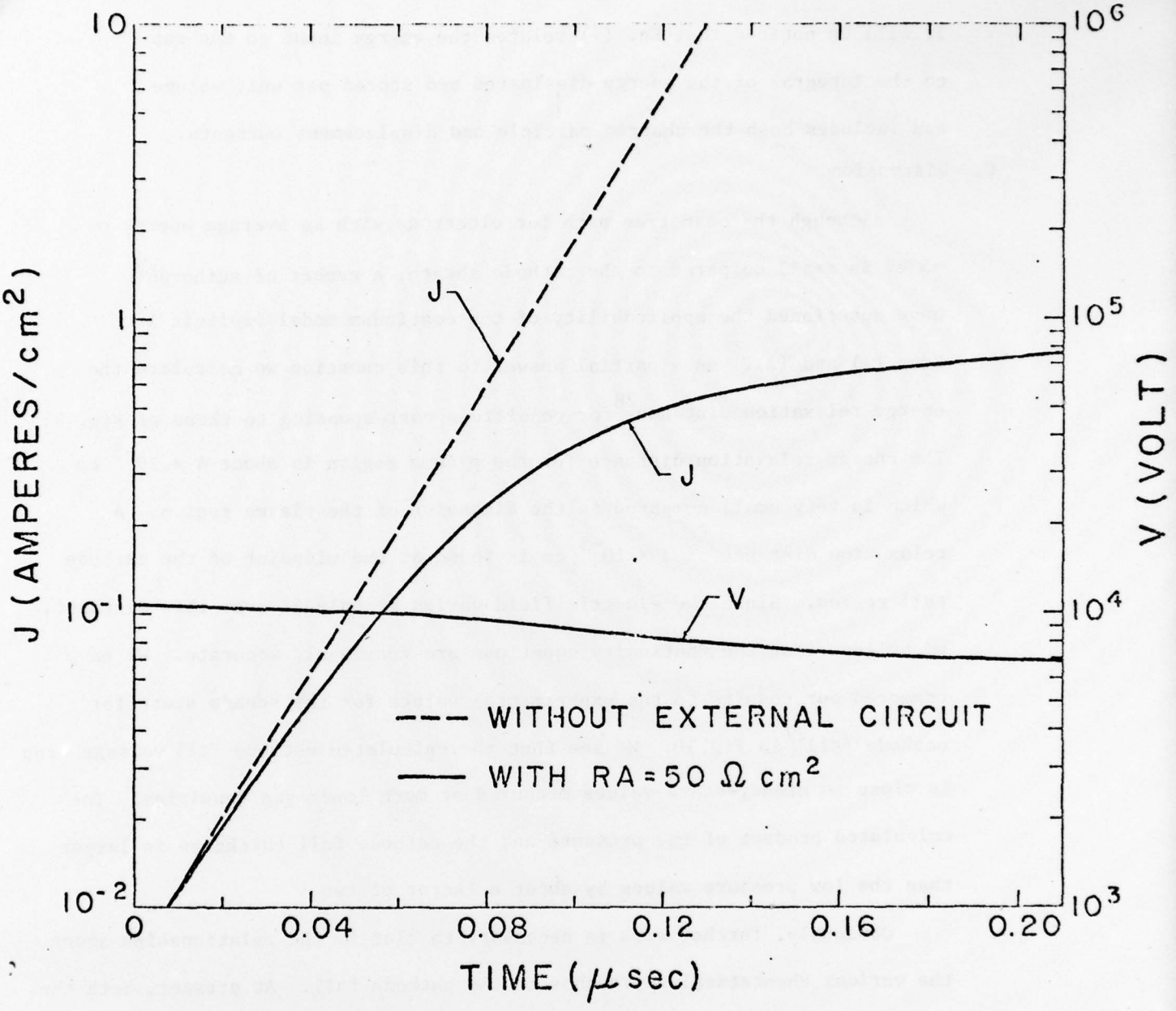

Fig. 9. Current and voltage transients. The dashed curve is calculated from the profiles of Figs. 5-8, while the solid curve is calculated using a resistance times area value of 50 Ω-cm^2.

It will be noticed that Eq. (7) relates the energy input to the gap to the integral of the energy dissipated and stored per unit volume and includes both the charged particle and displacement currents.

C. Discussion

Although the mean free path for electrons with an average energy of ~5 eV is small compared to the cathode sheath, a number of authors[27] have questioned the applicability of the continuum model implicit in Eqs. (1) and (2). As a partial answer to this question we calculate the energy relaxation distance[28] for conditions corresponding to those of Fig. 8. The energy relaxation distance for the plasma region is about 4×10^{-5} cm which is very small compared to the dimension of the plasma region. A relaxation distance of 3×10^{-5} cm is found at the midpoint of the cathode fall region. Since the electric field varies by only 4% over this distance, we believe that the continuity equations are reasonably accurate. We have compared our results to the experimental values for the steady state for cathode fall[29] in Fig. 10. We see that the calculated cathode fall voltage drop is close to steady-state values measured at much lower gas densities. The calculated product of the pressure and the cathode fall thickness is larger than the low pressure values by about a factor of two.

Obviously, further work is necessary to clarify the relationships among the various theoretical approaches to the cathode fall. At present, both the continuum model and the nearly free fall approaches seem to be able to use their methods to show their validity. In addition, other processes should be included in the model, e.g., the destruction and ionization of metastable atoms and molecules and the heating and subsequent motion of the neutral gas.[30]

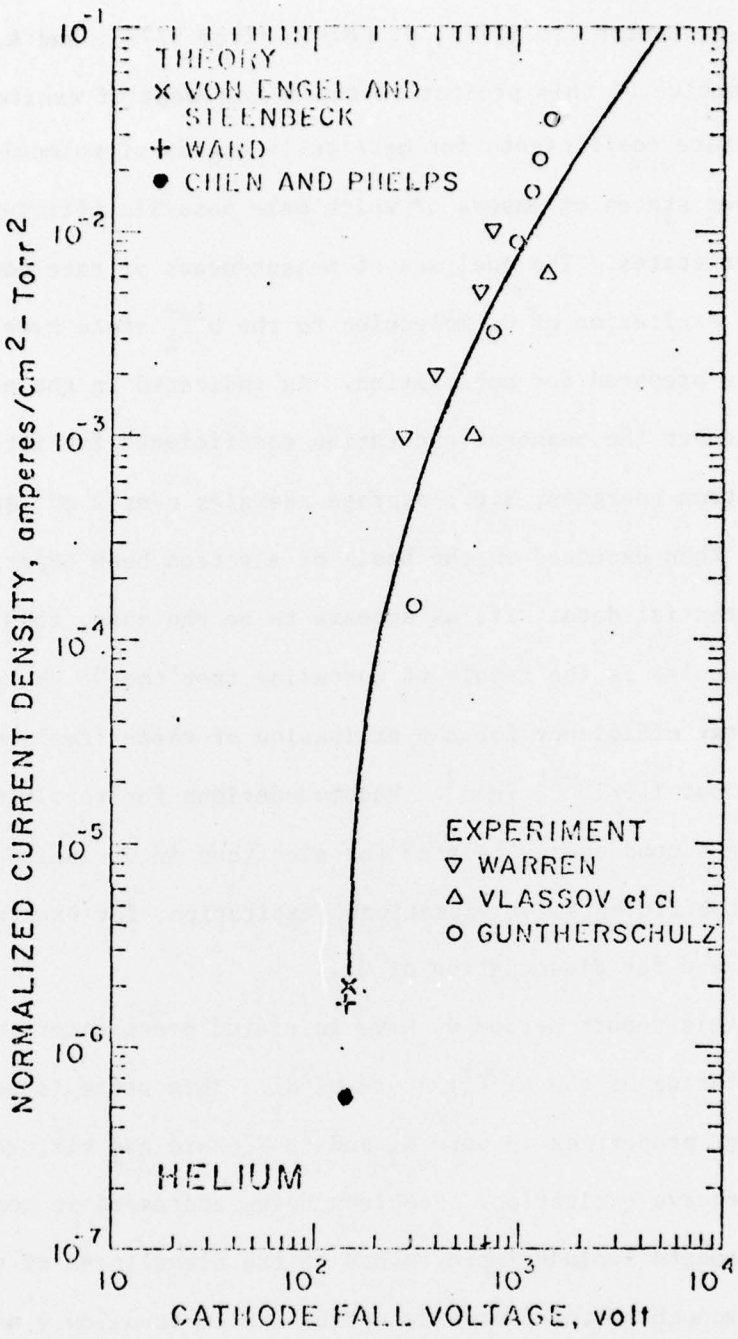

Fig. 10. Experimental and theoretical values of steady-state voltage drop across the cathode fall. The solid point is the result of our calculations using the delayed onset of ionization. The curve serves to connect the experimental and theoretical data.

IV. ELECTRON EXCITATION OF MOLECULAR METASTABLES

Drs. S. A. Lawton (to 9/77), D. Levron (from 9/77), and A. V. Phelps.

The objective of this project is the measurement of excitation and destruction rate coefficients for metastable states of molecules which serve as upper states of lasers or which make possible efficient excitation of such laser states. The analyses of measurements of rate coefficients for the electron excitation of O_2 molecules to the $b^1\Sigma_g^+$ state have been completed and are being prepared for publciation. As indicated in the previous Semiannual Report the measured excitation coefficients for intermediate electron energies, i.e., average energies near 2 eV, are a factor of three larger than expected on the basis of electron beam experiments and molecular potential data. If, as appears to be the case, this excitation of the $b^1\Sigma_g^+$ molecules is the result of cascading from the "6 eV levels" then the energy efficiency for the excitation of these levels must be near 60% for E/N of about 1.5×10^{-16} V-cm^2. Recommendations for resolving this discrepancy and providing a good energy balance for electrons in O_2 include measurement of the rate coefficients for vibrational excitation, for excitation of the $O_2\ ^1\Delta_g$ state, and for dissociation of O_2.

During this report period we have initiated measurements of rate coefficients for the excitation of the $A(^3\Sigma_U^+)$ state of N_2. This state is well known for its energy storage properties in pure N_2 and in N_2-rare gas mixtures under electron-beam and discharge excitation. Problems being addressed in connection with these measurements include improvements in the cleanliness of the vacuum system, a low noise monochromator-photon detection system to allow a measurement of the distribution of emitted radiation in the various ultraviolet and visible bands of N_2, a reduction in the intensity of scattered radiation from the uv source used to provide the photoelectrons used in the drift tube, and the absolute calibration of the photon detection system at the ultraviolet wavelengths emitted by the $A(^3\Sigma_u^+)$ metastables, i.e., the Vegard-Kaplan bands.

V. SCATTERING AND TRANSPORT OF RESONANCE RADIATION

Drs. T. Fujimoto (to 9/77), A. Zajonc (from 9/77), and A. V. Phelps.

The objective of this project is to determine the rates for both radiative and non-radiative energy loss from resonance states of a typical metal vapor atom (Na). The data resulting from such measurements are necessary for accurate modeling of proposed high power metal vapor-rare gas excimer lasers.

During this report period we have completed measurements and most of the analysis of the spectral intensity of scattered resonance radiation when Na vapor is excited with white light. With this mode of excitation the incident radiation excites atoms throughout the cell and the dominant loss processes are radiative transport and quenching by Na_2 and by any added gas, i.e., by N_2 in some of these experiments. Representative spectral intensity curves are shown for pure Na in Fig. 11, where the upper curve is the forward scattering and the lower curve is backward scattering. The points are measured values and the solid curves of Fig. 11 are the results of calculations using theory developed previously [D. G. Hummer and P. B. Kunasz, J. Quant. Spectrosc. and Radiat. Transfer 16, 77 (1976)] for the interpretation of these experiments and include the smearing effects of the measured monochromator profile. One notes that the agreement between theory and experiment is very good except at line center for the forward scattering. The origin of this discrepancy is unknown, although it could be an underestimate of the non-radiative transport of excitation to the entrance window.

In order to obtain a quantitative measure of the non-radiative contribution to the loss of resonance atoms, we have initiated measurements of the scattering of resonance radiation under conditions designed to emphasize the effects of non-radiative transport. The new feature is the use of monochromatic

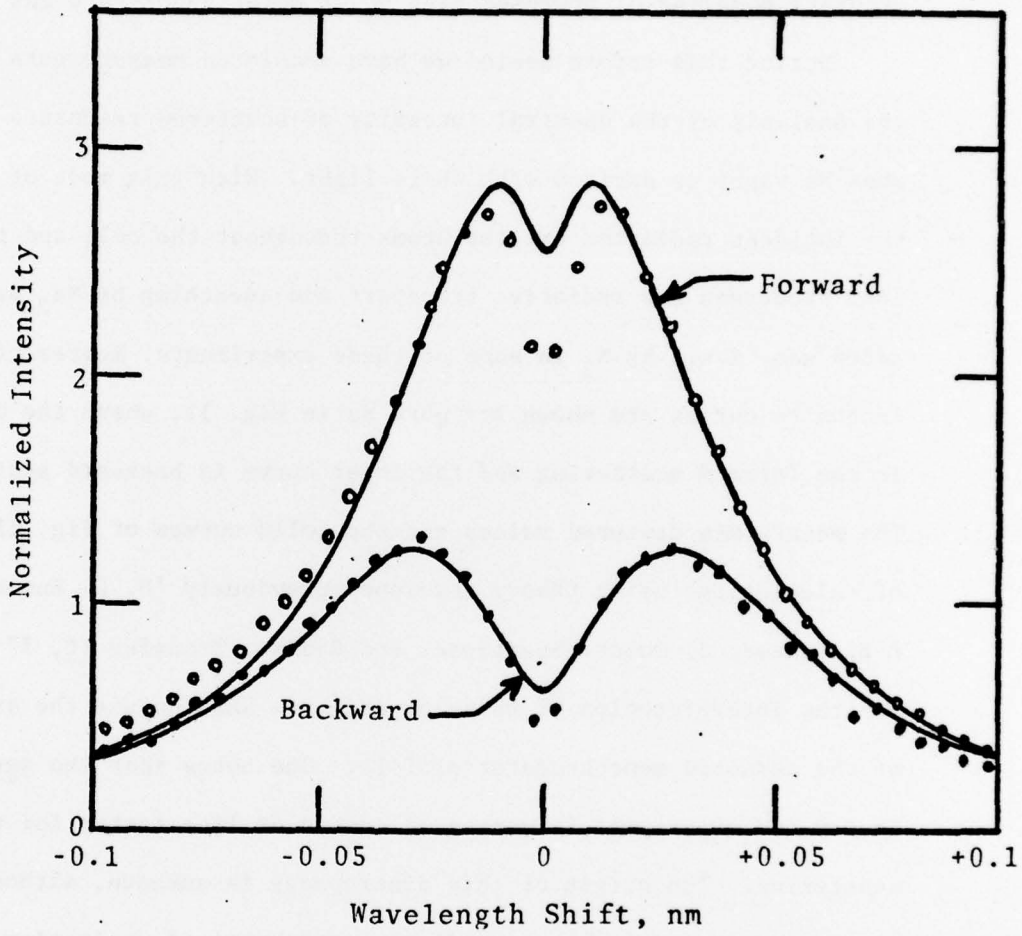

Fig. 11. Spectral intensity of forward and backward scattered resonance radiation from Na vapor illuminated by white light. The points are experiment and the lines are theory. [Na] = 5.3×10^{15} cm^{-3}. λ_o = 589.0 nm.

radiation rather than the white light source used previously. Since the absorption coefficient is very large at line center this method of excitation enables one to establish a large gradient in the excited atom density. Diffusive effects are expected to be important under such conditions. To this end a single-mode argon-ion pumped tunable CW dye laser has been made ready for use.

Previous measurements on the radiative and non-radiative transport of resonance radiation have been limited to temperatures below 500 C ($[Na] \lesssim 5\times10^{16}$ cm^{-3}). Since non-radiative transport becomes more important at high vapor densities, work is presently underway to extend these measurements to densities as high as 10^{18} cm^{-3}. Because of the difficulties encountered previously with "brazed" sapphire-metal seals and a welded cell construction, we are attempting to develop pressure seals with a thin metal gasket between the sapphire window and the cell body. This type of construction, of course, requires careful design and construction of the cell components with regard to coefficients of expansion and surface finish. A prototype sodium cell is presently undergoing testing.

REFERENCES

1. R. Shuker, A. V. Phelps and A. C. Gallagher, in Third Colloquium on Electronic Transition Lasers Snowmass, 1976, edited by J. Steinfeld (MIT Press, in press); R. Shuker, L. Morgan, A. C. Gallagher, and A. V. Phelps, Final Report Contract E(49-1)-3800, for July 1, 1975 to Sep. 30, 1976.
2. G. York and A. Gallagher, "High Power Gas Lasers Based on Alkali-dimer A-X Band Radiation," JILA Rept. 114 (1974) Joint Institute for Laboratory Astrophysics, University of Colorado, Boulder, CO 80309.
3. A. V. Phelps, "Tunable Gas Lasers Utilizing Ground State Dissociation," JILA Rept. 110 (1972), Joint Institute for Laboratory Astrophysics, University of Colorado, Boulder, CO 80309.
4. C. K. Rhodes, IEEE J. Quantum Electron. QE-10, 153 (1974).
5. A. J. Palmer, J. Appl. Phys. 47, 3088 (1976).
6. L. Schlie, J. Appl. Phys. 47, 1397 (1976).
7. D. Leep, H. Rothwell and A. Gallagher (unpublished).
8. G. York, R. Scheps and A. C. Gallagher, J. Chem. Phys. 63, 1052 (1975).
9. L. Lam, A. C. Gallagher and M. Hessel, J. Chem. Phys. 66, 3550 (1977).
10. D. L. Moores and D. W. Norcross, J. Phys. B 5, 1482 (1972); D. L. Moores, D. W. Norcross and V. B. Sheorey, J. Phys. B 7, 371 (1974).
11. E. Enemark and A. Gallagher, Phys. Rev. 6, 192 (1972).
12. S. J. B. Corrigan, J. Chem. Phys. 43, 4381 (1965).
13. S. Chung, C. C. Lin and E. T. P. Lee, Phys. Rev. A 6, 988 (1972).
14. M. Inokuti, Rev. Mod. Phys. 43, 297 (1971).
15. S. T. Chen and A. Gallagher, Phys. Rev. A 14, 593 (1976).
16. D. Norcross and D. J. Hummer, Bull. Am. Phys. Soc. 22, xxx (1977).
17. W. J. Stevens, M. M. Hessel, P. J. Bertoncini and A. C. Wahl, J. Chem. Phys. 66, 1477 (1977).

18. R. Scheps and A. Gallagher, J. Chem. Phys. 65, 859 (1976).

19. See, for example, W. W. Rigrod, J. Appl. Phys. 36, 2487 (1965).

20. See, for example, L. M. Biberman, V. S. Vorob'ev and I. T. Yakubov, Uspeki Fizicheskikh Nauk 107, 353 (1972) [Translation: Soviet Physics-Uspekhi 15, 375 (1973)].

21. J. L. Ward, J. Appl. Phys. 33, 2789 (1962). See also M. Nahemow, N. Wainfan and A. L. Ward, Phys. Rev. 137, A56 (1965).

22. L. E. Kline, J. Appl. Phys. 45, 2046 (1974) and 46, 1567 (1975).

23. C. B. Mills, J. Appl. Phys. 45, 2112 (1974).

24. E. F. Jaeger, L. Oster, and A. V. Phelps, Phys. Fluids 19, 819 (1976).

25. M. J. Druyvesteyn and F. M. Penning, Rev. Mod. Phys. 12, 87 (1940).

26. R. D. Richtmyer and K. W. Morton, Difference Methods for Initial Value Problems (Interscience, New York, 1967).

27. W. P. Allis, Revue de Phys. Appliquée 10, 97 (1975).

28. J. J. Lowke and D. K. Davies, Westinghouse Reserach Laboratories, Scientific Paper 72-108-ARCPL-P4 (unpublished). For the conditions of the present calculation, the formulas of this reference give an energy relaxation distance, λ_ε, of $\lambda_\varepsilon = D/\mu E$.

29. J. D. Cobine, Gaseous Conductors (Dover, New York, 1958).

30. The calculated rate of heat input near the center of the cathode fall using the results shown in Fig. 4 is 1 mw/cm^3 or 2.3×10^5 eV/atom-sec. This corresponds to a temperature rise of about 250 K in 100 nsec. A sound wave would travel through the cathode fall region in about 10 nsec. The expanding low density region produced by heating in the cathode fall region has been observed experimentally.

For example, Crawford and Phelps (unpublished) have made interferometric observations of this region and Rogoff has calculated some of its properties. See also, E. R. Pugh, J. Wallace, J. H. Jacob, D. B. Northam, Applied Optics 13, 2512 (1974); F.E.C. Culick, P. I. Shen and W. S. Griffen, IEEE J. Quantum Electron. QE-12, 566 (1976).